Available online at www.sciencedirect.com

ScienceDirect

Ceramics International 39 (2013) 9009–9015

CERAMICS INTERNATIONAL

www.elsevier.com/locate/ceramint

Improvement on the phase stability, mechanical properties and thermal insulation of Y_2O_3-stabilized ZrO_2 by Gd_2O_3 and Yb_2O_3 co-doping

Lei Guo[a,b], Hongbo Guo[a,b,*], Shengkai Gong[a,b], Huibin Xu[a,b]

[a]School of Materials Science and Engineering, Beihang University, No. 37, Xueyuan Road, Beijing 100191, China
[b]Beijing Key Laboratory for Advanced Functional Material and Thin Film Technology, Beihang University, No. 37, Xueyuan Road, Beijing 100191, China

Received 27 March 2013; received in revised form 27 April 2013; accepted 28 April 2013
Available online 4 May 2013

Abstract

Gd_2O_3 and Yb_2O_3 co-doped 3.5 mol% Y_2O_3–ZrO_2 and conventional 3.5 mol% Y_2O_3–ZrO_2 (YSZ) powders were synthesized by solid state reaction. The objective of this study was to improve the phase stability, mechanical properties and thermal insulation of YSZ. After heat treatment at 1500 °C for 10 h, 1 mol% Gd_2O_3–1 mol% Yb_2O_3 co-doped YSZ (1Gd1Yb-YSZ) had higher resistance to destabilization of metastable tetragonal phase than YSZ. The hardness of 5 mol% Gd_2O_3–1 mol% Yb_2O_3 co-doped YSZ (5Gd1Yb-YSZ) was higher than that of YSZ. Compared with YSZ, 1Gd1Yb-YSZ and 5Gd1Yb-YSZ exhibited lower thermal conductivity and shorter phonon mean free path. At 1300 °C, the thermal conductivity of 5Gd1Yb-YSZ was 1.23 W/m K, nearly 25% lower than that of YSZ (1.62 W/m K). Gd_2O_3 and Yb_2O_3 co-doped YSZ can be explored as a candidate material for thermal barrier coating applications.

Keywords: C. Mechanical properties; C. Thermal conductivity; D. ZrO_2; E. Thermal applications

1. Introduction

The application of thermal barrier coatings (TBCs) on hot components of gas turbines enables increase in overall engine efficiency by either lowering the metal surface temperature or maintaining the existing metal surface temperatures by decreasing cooling air flow [1,2]. Currently, the material of choice for TBCs is 6–8 wt% Y_2O_3 stabilized ZrO_2 (YSZ), which exhibits metastable tetragonal (t′) form when applied on superalloy components by plasma spraying or by electron-beam physical vapor deposition (EB-PVD) [3–5]. However, t′ phase becomes increasingly unstable at high temperatures, it decomposes to a mixture of tetragonal (t) and cubic (c) phases. On cooling t phase transforms to monoclinic (m) phase, accompanied with excessive volume expansion, resulting in crack formation in TBCs [3–5]. Demand for enhanced jet engine efficiencies necessitates significant increase in combustion temperatures and operating pressures. To cope with these requirements, alternate TBCs materials are strongly required having higher temperature capability, better mechanical properties and lower thermal conductivity.

In order to search for alternate TBCs materials, efforts have been made in two approaches: (1) alternate materials to ZrO_2-based systems, and (2) alternate stabilizers to Y_2O_3 for ZrO_2-based systems. The former includes pyrochlore-structured materials [6–8], fluorite-structured materials [9,10], perovskite-structured materials [11,12] and magnetoplumbite lanthanum hexaaluminate [13,14]. The latter is more relevant to the experiments described in the present study.

Maintenance of t′ phase in ZrO_2-based materials is crucial to the durability of TBCs not only because t′ phase has low intrinsic thermal conductivity, but also because of its high toughness. To improve the high temperature capability of t′ phase in YSZ, single stabilizers or co-dopants were used to partially or completely substitute Y_2O_3 in YSZ. Rebollo and Fabrichnaya [15,16] reported that the phase stability of t′ phase in 3.8 mol% Y_2O_3+3.8 mol% RE_2O_3 (RE=Yb, Gd, Sm, and

*Corresponding author at: School of Materials Science and Engineering, Beihang University, No. 37, Xueyuan Road, Beijing 100191, China. Tel./fax: +86 10 8231 7117.
E-mail address: guo.hongbo@buaa.edu.cn (H. Guo).

0272-8842/$ - see front matter © 2013 Elsevier Ltd and Techna Group S.r.l. All rights reserved.
http://dx.doi.org/10.1016/j.ceramint.2013.04.103

Nd) co-doped ZrO_2 is better than that in YSZ. Yb_2O_3 doped YSZ was reported to have higher resistance for destabilization of t′ phase [17,18]. Sun et al. improved the phase stability of t′ phase in Sc_2O_3 stabilized ZrO_2 by partial substituting Sc_2O_3 with Gd_2O_3 [19]. Gd_2O_3 and Yb_2O_3 seem to have good performance on improving the t′ phase stability, however, no report was published on the effects of Gd_2O_3 and Yb_2O_3 co-doping on the phase stability of t′ phase in YSZ. Zhu et al. reported that doping two or more additives to YSZ leads to a lower thermal conductivity [20]. In our previous work, 3 mol% Gd_2O_3 and 3 mol% Yb_2O_3 co-doped YSZ was found to exhibit much lower thermal conductivity than YSZ [21]. Gd–O bond was calculated to have the lowest bond population among the RE–O bonds (RE=rare earth elements), which indicates that Gd_2O_3 doping can reduce thermal conductivity effectively [22]. Therefore, increasing Gd_2O_3 content in Gd_2O_3 and Yb_2O_3 doped YSZ can lead to lower thermal conductivity. In this study, Gd_2O_3 and Yb_2O_3 co-doped YSZ was synthesized by solid state reaction. The effects of Gd_2O_3 and Yb_2O_3 co-doping on the phase stability, mechanical properties and thermal conductivity of YSZ were investigated. The data was compared with that for 3.5 mol% Y_2O_3-doped ZrO_2 produced by a similar technique.

2. Experimental procedure

Powders of 1 mol% Gd_2O_3–1 mol% Yb_2O_3 co-doped 3.5 mol % Y_2O_3–ZrO_2 (1Gd1Yb-YSZ), 5 mol.% Gd_2O_3–1 mol% Yb_2O_3 co-doped 3.5 mol% Y_2O_3–ZrO_2 (5Gd1Yb-YSZ) and baseline 3.5 mol% Y_2O_3–ZrO_2 (YSZ) were synthesized by the solid sate reaction method. Gd_2O_3, Yb_2O_3, Y_2O_3 and ZrO_2 powders were used as raw materials, which were pre-calcined at 900 °C for 4 h to remove adsorptive water and/or carbon dioxide before weighting. The appropriate amounts of individual oxides were dissolved in ionized water and mechanically milled for 10 h. The mixed powders were then calcined at 1400 °C for 12 h. The bulk materials were produced by hot pressing with a pressure of 20 MPa at 1400 °C for 2 h.

Phase composition analysis was conducted by X-ray diffraction (XRD, Rigaku Diffractometer, CuKα radiation). The phase stability of t′ phase in the synthesized powders was studied by annealing the powders at 1500 °C for 10 h. The mole fractions of m-ZrO_2 (M_m) and c/t′-ZrO_2 ($M_{c,t'}$) were determined from XRD using the most common equation [23]:

$$\frac{M_m}{M_{c,t'}} = 0.82\frac{I_m(\bar{1}11) + I_m(111)}{I_{c,t'}(111)} \quad (1)$$

where $I_m(\bar{1}11)$ and $I_m(111)$ are the X-ray diffraction intensities reflected from the $(\bar{1}11)$ and (111) planes of m-ZrO_2, respectively, and $I_{c,t'}(111)$ is the diffraction intensity reflected from the (111) plane of c/t′-ZrO_2.

The microstructure of bulk materials was observed by a scanning electron microscope (SEM, FEI, Holland) equipped with energy dispersive spectroscopy (EDS, IE 350). The Knoop indentations were performed on bulk ceramics at a load of 500 g for 20 s using a microhardness tester (HXZ-1000, China). At least 10 valid indentations were made for each sample. The Knoop hardness (H_K) was calculated according to the following equation [24]:

$$H_K = \frac{14.229\,P}{d^2} \quad (2)$$

where P is the test load (Kg), d is the length of the long indentation diagonal (mm). Young's modulus (E) was determined using the following equation [25]:

$$\frac{b'}{a'} = \frac{b}{a} - \alpha\frac{H_K}{E} \quad (3)$$

where b/a is the ratio of the short diagonal and the long diagonal of each indentation, b'/a' is the ratio of the short diagonal and the long diagonal of the indentation after elastic recovery. H_K and E are the Knoop hardness and Young's modulus, respectively. The constant α has a value of 0.45.

The thermal diffusivity (λ) was measured by laser flash device (Netzsch LFA427, Germany) from 25 °C to 1300 °C. The sample for thermal diffusivity measurement has a dimension of 12.7 mm in diameter and 1 mm in thickness. Prior to the thermal diffusivity measurement, the surfaces of the specimen were coated with a thin layer of graphite for thermal absorption of laser pulses. Thermal diffusivities of all samples were measured three times at each temperature. The specific heat capacity (C_p) was calculated from the specific heat capacity data of constituent oxides according to the Neumann–Kopp rule [26]. The bulk density (ρ) was measured by the Archimedes method. The thermal conductivity (κ) was calculated by the following equation:

$$\kappa = \lambda C_p \rho \quad (4)$$

Because the sintered samples were not fully dense, the measured thermal conductivity values were corrected for the actual data (κ_0) using the following equation [27]:

$$\frac{\kappa}{\kappa_0} = 1 - \frac{4}{3}\varphi \quad (5)$$

where φ is the fractional porosity.

3. Results and discussion

Fig. 1 shows the XRD patterns of YSZ, 1Gd1Yb-YSZ and 5Gd1Yb-YSZ powders synthesized at 1400 °C for 12 h. All the samples only exhibit zirconia phase, indicating that dopants have been dissolved into ZrO_2 crystal. Diffraction peak at $2\theta \approx 34°$ is found in YSZ and 1Gd1Yb-YSZ, which is the characteristic peak of t′ phase. YSZ and 1Gd1Yb-YSZ consist of c, t′ and m phases, while 5Gd1Yb-YSZ is composed of c and m phases. The m phase in the powders is formed due to phase transformation. At the synthesized temperature (1400 °C), YSZ is composed of c and t phases. The t phase transforms to m phase upon cooling unless the cooling rate is very fast. It is known that YSZ TBCs produced by EB-PVD and plasma spraying mostly consist of t' phase, and very limited amount of m phase is formed, which is attributed to the extremely fast cooling rate during the coating fabrication process. The XRD patterns of YSZ, 1Gd1Yb-YSZ and 5Gd1Yb-YSZ powders after heat treatment at 1500 °C for 10 h are shown in Fig. 2. The phase constitution of each sample

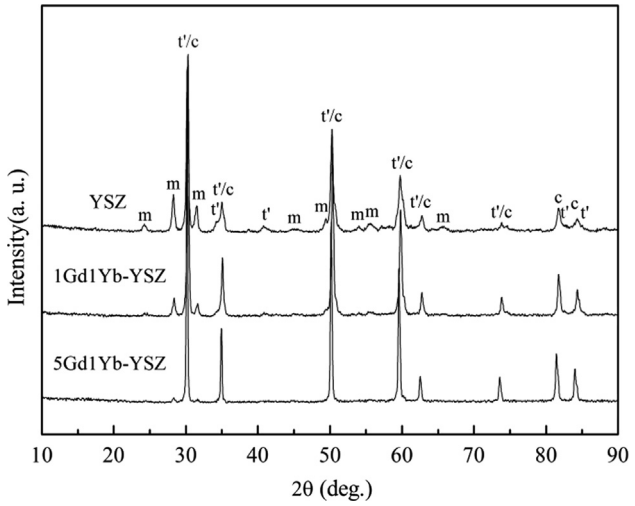

Fig. 1. XRD patterns of YSZ, 1Gd1Yb-YSZ and 5Gd1Yb-YSZ powders synthesized at 1400 °C for 12 h.

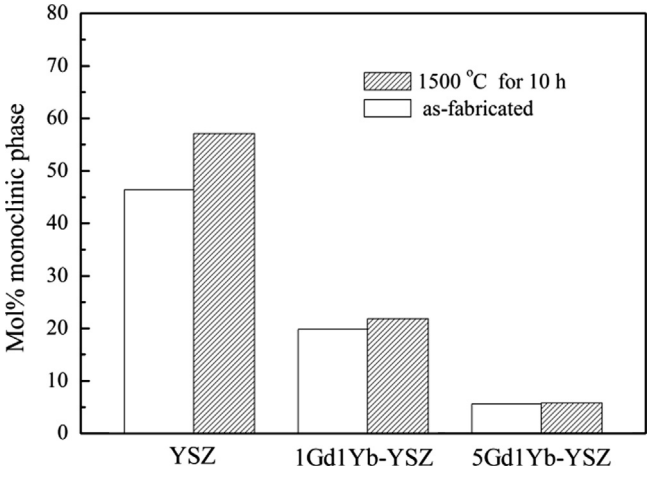

Fig. 3. Concentrations (in mol%) of monoclinic phase determined from XRD for YSZ, 1Gd1Yb-YSZ and 5Gd1Yb-YSZ powders.

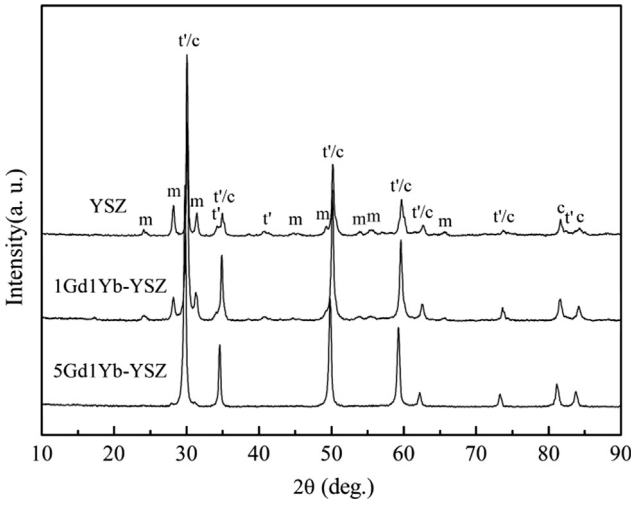

Fig. 2. XRD patterns of YSZ, 1Gd1Yb-YSZ and 5Gd1Yb-YSZ powders after heat treatment at 1500 °C for 10 h.

does not change after heat treatment, but m phase contents increase in different extents for the three samples.

The concentration of m phase calculated using Eq. (1) is shown in Fig. 3. After heat treatment at 1500 °C for 10 h, m phase content of 5Gd1Yb-YSZ almost keeps constant, while those of YSZ and 1Gd1Yb-YSZ increase. It is known that m phase transforms to t phase on heating and on cooling t phase transforms to m phase, during which about 3.5% volume change occurs [4,28]. Due to the volume change, the phase transformation is accompanied by the formation of small cracks around the transformed particle, these cracks greatly increase the energy absorbed during crack extension, and thus improve the toughness of the material [29,30]. However, excessive phase transformation reduces the mechanical properties, therefore, m phase content in TBCs materials should be low. The m phase contents in 5Gd1Yb-YSZ before and after heat treatment are 5.6% and 5.8%, respectively. A small amount of m phase in ZrO_2-based materials is beneficial to improve mechanical properties, giving rise to longer lifetime when the material is used as TBCs. The m phase contents of YSZ and 1Gd1Yb-YSZ increase from 46.4% to 57.1% and from 19.8% to 21.8%, respectively, which can be attributed to the partitioning of t′ phase. At high temperatures, t′ phase undergoes a diffusion-controlled partitioning to c phase and t phase, with t phase transforming to m phase on cooling [3,31]. The presence of t′ phase is beneficial to the durability of materials used as TBCs due to its high toughness [32]. The increasing degrees of m phase contents for YSZ and 1Gd1Yb-YSZ are 23.1% and 10.1%, respectively, which indicates that Gd_2O_3 and Yb_2O_3 co-doping can improve the resistance to destabilization of t′-ZrO_2 in YSZ.

Fig. 4 shows the typical fracture morphologies of YSZ, 1Gd1Yb-YSZ and 5Gd1Yb-YSZ bulk ceramics. All the samples exhibit intergranular fracture. From SEM observations, there are some small pores in the ceramics. The grain boundaries of YSZ and 1Gd1Yb-YSZ bulk ceramics are clearly visible, while the grain boundaries of 5Gd1Yb-YSZ bulk ceramics exhibit a little blurry however, each grain can be easily distinguished. The average grain size of YSZ and 1Gd1Yb-YSZ bulk ceramics is 1–3 μm, while that of 5Gd1Yb-YSZ bulk ceramics is 3–5 μm.

Fig. 5 shows the Knoop indentation impressions of YSZ, 1Gd1Yb-YSZ and 5Gd1Yb-YSZ bulk ceramics with an applied load of 500 g. The indentation tips in the three ceramics can be clearly seen and no crack is found. The Knoop hardness was obtained by using Eq. (2), and the results are shown in Fig. 6. The values for Knoop hardness of 1Gd1Yb-YSZ and 5Gd1Yb-YSZ are 7.3 GPa and 8.4 GPa, respectively, which are higher than that of YSZ (6.5 GPa), indicating that Gd_2O_3 and Yb_2O_3 co-doping increases the Knoop hardness of YSZ. High hardness is desirable for materials used as TBCs, it can improve the resistance of the coatings to erosion and thus improve the coatings lifetime [28]. The a'/b' values of YSZ, 1Gd1Yb-YSZ and 5Gd1Yb-YSZ are 8.54, 8.49, and 8.46, respectively, which were obtained by

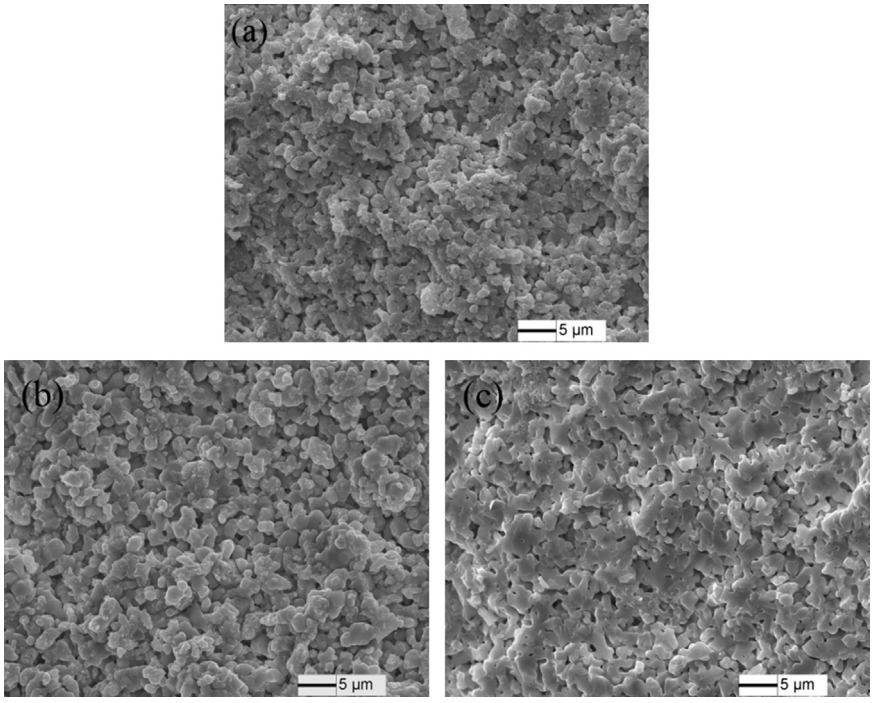

Fig. 4. Fracture morphologies of YSZ (a), 1Gd1Yb-YSZ (b) and 5Gd1Yb-YSZ (c) bulk ceramics.

averaging the results of 10 Knoop indentations in each sample. According to Eq. (3), Young's modulus can be calculated, and the results are also presented in Fig. 6. Young's modulus of YSZ is 124.5 GPa, while those of 1Gd1Yb-YSZ and 5Gd1Yb-YSZ are 143.8 GPa and 168.5 GPa, respectively. It has been reported that the ratio of hardness versus elastic modulus (H_K/E) can be considered as a brittleness index, a higher ratio value means a higher brittleness of the material [33,34]. The values of H_K/E of YSZ, 1Gd1Yb-YSZ and 5Gd1Yb-YSZ are 0.052, 0.051 and 0.050 respectively, which indicates a slight increase in the toughness of YSZ with the additions of Gd_2O_3 and Yb_2O_3.

Fig. 7 shows the thermal diffusivities of YSZ, 1Gd1Yb-YSZ and 5Gd1Yb-YSZ. All the samples reveal a decline tendency in thermal diffusivities with temperature rising from 25 °C to 1300 °C. The thermal diffusivities of the doped specimens are relatively lower than those of YSZ. At 1300 °C, the thermal diffusivities of YSZ, 1Gd1Yb-YSZ and 5Gd1Yb-YSZ are 0.39 mm^2/s, 0.37 mm^2/s and 0.30 mm^2/s, respectively. The thermal conductivities were calculated based on Eq. (4) and the results were calibrated according to Eq. (5) to represent full dense samples, as shown in Fig. 8. The thermal conductivities of YSZ, 1Gd1Yb-YSZ and 5Gd1Yb-YSZ are in the ranges of 1.62–2.12 W/m K, 1.53–1.84 W/m K and 1.23–1.32 W/m K, respectively. Gd_2O_3 and Yb_2O_3 co-doping reduces the thermal conductivity of YSZ. At 1300 °C, the thermal conductivity of 5Gd1Yb-YSZ is 1.23 W/m K, nearly 25% lower than that of YSZ (1.62 W/m K). The low thermal conductivity of material is beneficial to improve the thermal insulation property when applied on superalloy components such as blades, vanes and combustors.

In order to understand the effects of Gd_2O_3 and Yb_2O_3 co-doping on the thermal conductivity of YSZ, we refer to Debye's phonon gas theory, in which heat conduction process was considered as energy exchange between phonons [35]:

$$\kappa = \frac{1}{3} C_p l_p \rho v \tag{6}$$

where C_p, l_p and ν represent the heat capacity per unit volume, the phonon mean free path and the sound speed, respectively. The sound speed (ν) is defined by the following equation [5]:

$$v = 0.87\sqrt{\frac{E}{\rho}} \tag{7}$$

By combining Eqs. (4) and (6), the phonon mean free path can be written as

$$l_p = 3\alpha/\nu \tag{8}$$

The phonon mean free path of YSZ, 1Gd1Yb-YSZ and 5Gd1Yb-YSZ versus temperature was plotted in Fig. 9. It can be found that phonon mean free path of these samples decreases with temperature rising from 25 °C to 1300 °C. Gd_2O_3 and Yb_2O_3 co-doping reduces the phonon mean free path of YSZ, implying that more phonon scattering resources exist in the doped YSZ. The phonon mean free path of 5Gd1Yb-YSZ was determined to be 2.91 nm at room temperature, nearly 45% shorter than that of YSZ (5.10 nm).

For an electrical insulting material, the phonon mean free path is determined by phonon–phonon scattering, defect scattering and grain boundary scattering [35]. In the present case, the grain boundary scattering can be ignored since the magnitude of phonon mean free path (~nm) is far smaller than that of grain size (~μm). Therefore, the reduction in phonon

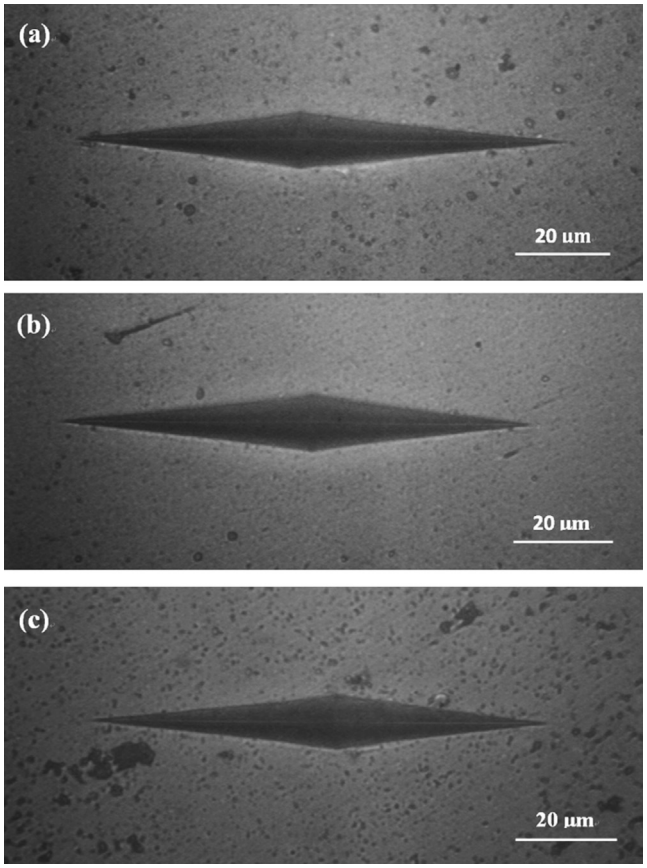

Fig. 5. Knoop indentation morphologies of YSZ (a), 1Gd1Yb-YSZ (b) and 5Gd1Yb-YSZ (c) bulk ceramics.

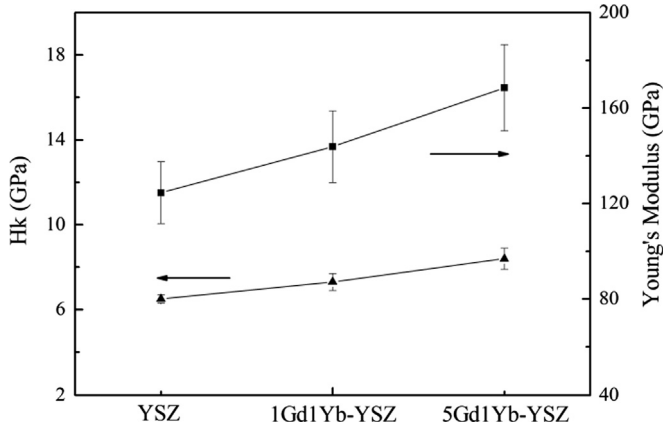

Fig. 6. Microhardness and Young's modulus of YSZ, 1Gd1Yb-YSZ and 5Gd1Yb-YSZ bulk ceramics.

mean free path of doped YSZ can be attributed to the increase in phonon scattering at defects. It is known that the ionic radii of Gd^{3+}, Yb^{3+} and Zr^{4+} are 1.06 Å, 0.98 Å and 0.72 Å respectively, and the atomic masses of Gd^{3+}, Yb^{3+} and Zr^{4+} are 157, 173 and 91 respectively. The substitutions of Gd^{3+} and Yb^{3+} for Zr^{4+} cause substitutional defects and extra oxygen vacancies, which enhance phonon scattering and thus reduce the phonon mean free path.

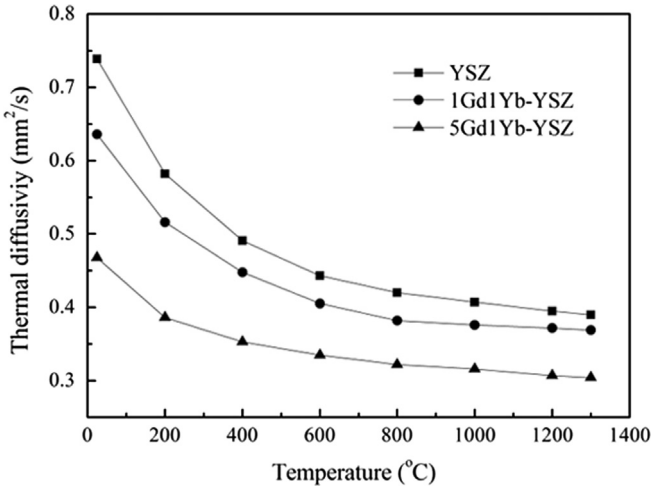

Fig. 7. Thermal diffusivities of YSZ, 1Gd1Yb-YSZ and 5Gd1Yb-YSZ.

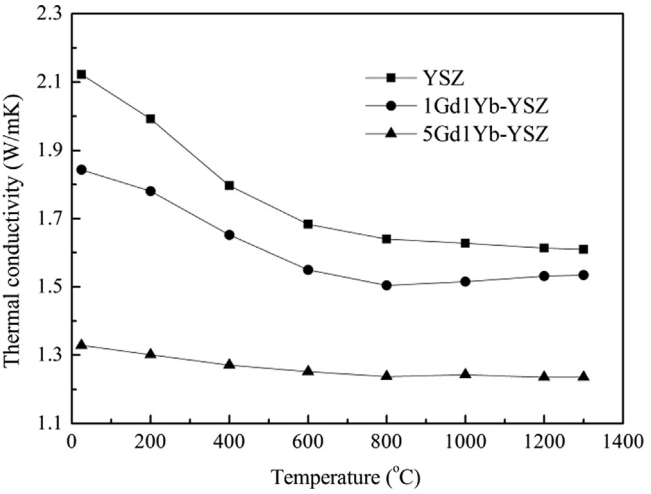

Fig. 8. Thermal conductivities of YSZ, 1Gd1Yb-YSZ and 5Gd1Yb-YSZ.

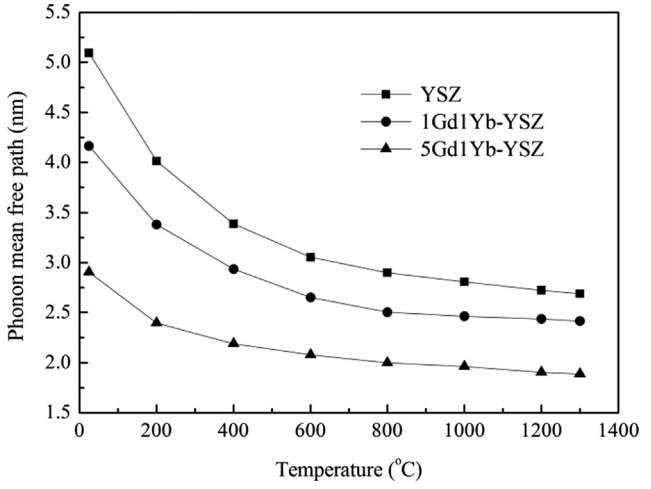

Fig. 9. Calculated phonon mean free path of YSZ, 1Gd1Yb-YSZ and 5Gd1Yb-YSZ.

4. Conclusions

Gd_2O_3 and Yb_2O_3 co-doped 3.5 mol% Y_2O_3–ZrO_2 and conventional 3.5 mol% Y_2O_3–ZrO_2 (YSZ) powders and bulk materials were produced by solid state reaction and hot pressing, respectively. Gd_2O_3 and Yb_2O_3 co-doping improved the phase stability, mechanical properties and thermal insulation of YSZ. 1 mol% Gd_2O_3–1 mol% Yb_2O_3 co-doped YSZ (1Gd1Yb-YSZ) had higher resistance to destabilization of metastable tetragonal phase than YSZ. The hardness and elastic modulus of YSZ increased with the additions of Gd_2O_3 and Yb_2O_3, 5 mol% Gd_2O_3–1 mol% Yb_2O_3 co-doped YSZ (5Gd1Yb-YSZ) exhibied relative higher toughness. Gd_2O_3 and Yb_2O_3 co-doped YSZ exhibited lower thermal conductivity and shorter phonon mean free path when compared with YSZ. The thermal conductivities of 1Gd1Yb-YSZ and 5Gd1Yb-YSZ were in the ranges of 1.53–1.84 W/m K and 1.23–1.32 W/m K, respectively, lower than those of YSZ (1.62–2.12 W/m K). The reduction in phonon mean free path of doped YSZ could be attributed to the stronger phonon scattering at defects which were increased by Gd^{3+} and Yb^{3+} substitution for Zr^{4+}. These merits propose Gd_2O_3 and Yb_2O_3 co-doped YSZ as a potential TBC material.

Acknowledgments

This research is sponsored by Nature Science Foundations of China (NSFC) under Grant nos. 51071013 and 51231001 and National Basic Research Program (973 Program) of China under Grant no. 2012CB625100.

References

[1] G.W. Goward, Progress in coatings for gas turbine airfoils, Surface and Coatings Technology 108–109 (1998) 73–79.
[2] A.M. Limarga, S. Shian, M. Baram, D.R. Clarke, Effect of high-temperature aging on the thermal conductivity of nanocrystalline tetragonal yttria-stabilized zirconia, Acta Materialia 60 (2012) 5417–5424.
[3] U. Schulz, Phase transformation in EB-PVD yttria partially stabilized zirconia thermal barrier coatings during annealing, Journal of the American Ceramic Society 83 (2000) 904–910.
[4] M.N. Rahaman, J.R. Gross, R.E. Dutton, H. Wang, Phase stability, sintering, and thermal conductivity of plasma-sprayed ZrO_2–Gd_2O_3 compositions for potential thermal barrier coating applications, Acta Materialia 54 (2006) 1615–1621.
[5] D.R. Clarke, Materials selection guidelines for low thermal conductivity thermal barrier coatings, Surface and Coatings Technology 163 (2003) 67–74.
[6] Z.G. Liu, J.H. Ouyang, Y. Zhou, J. Li, X.L. Xia, Influence of ytterbium- and samarium-oxides codoping on structure and thermal conductivity of zirconate ceramics, Journal of the European Ceramic Society 29 (2009) 647–652.
[7] Z.G. Liu, J.H. Ouyang, B.H. Wang, Y. Zhou, J. Li, Thermal expansion and thermal conductivity of $Sm_xZr_{1-x}O_{2-x/2}$ ($0.1 \le x \le 0.5$) ceramics, Ceramics International 35 (2009) 791–796.
[8] C.L. Wan, Z.X. Qu, A.B. Du, W. Pan, Influence of B site substituent Ti on the structure and thermophysical properties of $A_2B_2O_2$-type pyrochlore $Gd_2Zr_2O_7$, Acta Materialia 57 (2009) 4782–4789.
[9] W. Ma, S.K. Gong, H.F. Li, H.B. Xu, Novel thermal barrier coatings based on $La_2Ce_2O_7$/8YSZ double-ceramic-layer systems deposited by electron beam physical vapor deposition, Surface and Coatings Technology 202 (2008) 2704–2708.
[10] H.S. Zhang, J.G. Lv, G. Li, Z. Zhang, X.L. Wang, Investigation about thermophysical properties of $Ln_2Ce_2O_7$ (Ln = Sm, Er and Yb) oxides for thermal barrier coatings, Materials Research Bulletin 47 (2012) 4181–4186.
[11] L. Guo, H.B. Guo, G.H. Ma, M. Abbas, S.K. Gong, Ruddlesden–Popper structured $BaLa_2Ti_3O_{10}$, a highly anisotropic material for thermal barrier coatings, Ceramics International 38 (2012) 4345–4352.
[12] L. Guo, H.B. Guo, G.H. Ma, S.K. Gong, H.B. Xu, Phase stability, microstructural and thermo-physical properties of BaLn2Ti3O10 (Ln = Nd and Sm) ceramics, Ceramics International 39 (2013) 6743–6749.
[13] X.Y Xie, H.B. Guo, S.K. Gong, H.B. Xu, Lanthanum–titanium–aluminum oxide: a novel thermal barrier coating material for applications at 1300 °C, Journal of the European Ceramic Society 31 (2011) 1677–1683.
[14] M. Abbas, L. Guo, H.B. Guo, Evaluation of stress distribution and failure mechanism in lanthanum–titanium–aluminum oxides thermal barrier coatings, Ceramics International 39 (2013) 5103–5111.
[15] N.R. Rebollo, O. Fabrichnay, C.G. Levi, Phase stability of Y+Gd co-doped zirconia, Zeitschrift fur Metallkunde 94 (2003) 163–170.
[16] N.R. Rebollo, A.S. Gandhi, C.G. Levi, Phase stability issues in emerging TBC systems, in: E.J. Opila, P. Hou, T. Maruyama, B. Pieraggi, M. McNallan, D. Shifler, E. Wuchina (Eds.), High Temperature Corrosion and Materials Chemistry IV, Proceedings of the Electrochemical Society, vol. PV-2003-16, 2003, pp. 431–442.
[17] Y.M. Kan, S.L. Li, P.L. Wang, G.J. Zhang, O. Van der Biest, J. Vleugels, Preparation and conductivity of Yb_2O_3–Y_2O_3 and Gd_2O_3–Y_2O_3 co-doped zirconia ceramics, Solid State Ionics 179 (2008) 1531–1534.
[18] H.F. Liu, S.L. Li, Q.L. Li, Y.M. Li, W.X. Zhou, Microstructure, phase stability and thermal conductivity of plasma sprayed Yb_2O_3, Y_2O_3 co-stabilized ZrO_2 coatings, Solid State Sciences 13 (2011) 513–519.
[19] L.L Sun, H.B. Guo, H. Peng, S.K. Gong, H.B. Xu, Influence of partial substitution of Sc_2O_3 with Gd_2O_3 on the phase stability and thermal conductivity of Sc_2O_3-doped ZrO_2, Ceramics International 39 (2013) 3447–3451.
[20] D.M. Zhu, R.A. Miller, Development of advanced low conductivity thermal barrier coatings, International Journal of Applied Ceramic Technology 1 (2004) 86–94.
[21] Y.L. Zhang, L. Guo, Y.P. Yang, H.B. Guo, H.J. Zhang, S.K. Gong, Influence of Gd_2O_3 and Yb_2O_3 Co-doping on Phase Stability, thermophysical properties and sintering of 8YSZ, Chinese Journal of Aeronautics 25 (2012) 948–953.
[22] X.J. Ji, S.K. Gong, H.B. Xu, F.S. Liu, Influence of rare earth elements additions in YSZ ceramic coatings of thermal barrier coatings on lattice distortion, Acta Aeronautica et Astronautica Sinica 28 (2007) 196–200 (in Chinese).
[23] R.A. Miller, J.L. Smialek, R.G. Garlick, Phase stability in plasma sprayed partially stabilized zirconia-yttria, in: A.H. Heuer, A.L. Hobbs (Eds.), Advances in Ceramics, vol. 3, American Ceramic Society, Columbus, OH, 1981, pp. 241–253.
[24] P.J. Blau, Investigation of the nature of micro-indentation hardness gradients below sliding contacts in five copper alloys worn against 52100 steel, Journal of Materials Science 19 (1984) 1957–1968.
[25] D.B. Marshall, T. Noma, A.G. Evans, A simple method for determining elastic-modulus-to-hardness ratios using Knoop indentation measurements, Journal of the American Ceramic Society 65 (1982) C175–C176.
[26] O. Kubaschewski, C.B. Alcock, P.J. Spencer, Materials Thermochemistry, sixth ed., Pergamon Press, Oxford254–326.
[27] J. Wu, X.Z. Wei, N.P. Padture, P.G. Klemens, M. Gell, E. Garcia, P. Miranzo, M.I. Osendi, Low-thermal-conductivity rare-earth zirconates for potential thermal-barrier-coating applications, Journal of the American Ceramic Society 85 (2002) 3031–3035.
[28] X.Q. Cao, R. Vassen, D. Stoever, Ceramic materials for thermal barrier coatings, Journal of the European Ceramic Society 24 (2004) 1–10.
[29] T.K. Gupta, F. Lange, J. Bechtold, Effect of stress-induced phase transformation on the properties of polycrystalline zirconia containing metastable tetragonal phase, Journal of Materials Science 13 (1978) 1464–1470.

[30] Z. Ji, J. Haynes, M. Ferber, J. Rigsbee, Metastable tetragonal zirconia formation and transformation in reactively sputter deposited zirconia coatings, Surface and Coatings Technology 135 (2001) 109–117.
[31] R.A. Miller, R.G. Garlick, J. Smialek, Phase distributions in plasma-sprayed zirconia–yttria, American Ceramic Society Bulletin 62 (1983) 1355–1358.
[32] S. Stecura, Optimization of the NiCrAl–Y/ZrO_2–Y_2O_3 thermal barrier system, Advanced Ceramic Materials 1 (1986) 68–76.
[33] S.H. Leigh, C.K. Lin, C.C. Berndt, Elastic response of thermal spray deposits under indentation tests, Journal of the American Ceramic Society 80 (1997) 2093–2099.
[34] W. Wang, J. Liang, X. Guo, F. Xuan, H. Hong, Mechanical properties and dissolution behavior of plasma sprayed wollastonite coatings deposited at different substrate temperatures, Journal of Thermal Spray Technology 21 (2012) 496–504.
[35] R. Berman, Thermal Conduction in Solids, Clarendon Press, Oxford, 1976, pp. 45-101.